nanomaterials

MDPI

Article

Dopamine-Mediated Graphene Bridging Hexagonal Boron Nitride for Large-Scale Composite Films with Enhanced Thermal Conductivity and Electrical Insulation

Shikun Li [1,2,3], Yutan Shen [4], Xiao Jia [2,3], Min Xu [2,3], Ruoyu Zong [2,3], Guohua Liu [1], Bin Liu [2,3,*] and Xiulan Huai [2,3,*]

[1] Beijing Key Laboratory of Multiphase Flow and Heat Transfer for Low Grade Energy Utilization, North China Electric Power University, Beijing 102206, China; lishikun@iet.cn (S.L.); liuguohua126@126.com (G.L.)
[2] Institute of Engineering Thermophysics, Chinese Academy of Sciences, Beijing 100190, China; xumin@iet.cn (M.X.); zongruoyu@iet.cn (R.Z.)
[3] Nanjing Institute of Future Energy System, Nanjing 211135, China
[4] SINOPEC Research Institute of Petroleum Processing Co., Ltd., Beijing 100083, China; shenyutan.ripp@sinopec.com
* Correspondence: liubin@iet.cn (B.L.); hxl@iet.cn (X.H.)

Abstract: Heat accumulation generated from confined space poses a threat to the service reliability and lifetime of electronic devices. To quickly remove the excess heat from the hot spot, it is highly desirable to enhance the heat dissipation in a specific direction. Herein, we report a facile route to fabricate the large-scale composite film with enhanced thermal conductivity and electrical insulation. The well-stacked composite films were constructed by the assembly of polydopamine (PDA)-modified graphene nanosheets (GNS_{PDA}) and hexagonal boron nitride (BN_{PDA}), as well as bacterial cellulose (BC). The introduction of the PDA layer greatly improves the interface compatibility between hybrid fillers and BC matrix, and the presence of GNS_{PDA}-bridging significantly increases the probability of effective contact with BN_{PDA} fillers, which is beneficial to form a denser and complete "BN-GNS-BN" heat conduction pathway and tight filler–matrix network, as supported by the Foygel model fitting and numerical simulation. The resulting $BC/BN_{PDA}/GNS_{PDA}$ film shows the thermal conductivity and tensile strength of 34.9 $W \cdot m^{-1} \cdot K^{-1}$ and 30.9 MPa, which separately increases to 161% and 155% relative to the BC/BN_{PDA} film. It was found that the low electrically conductive and high thermal conductive properties can be well balanced by tuning the mass ratio of GNS_{PDA} at 5 wt%, and the electrical conductivity caused by GNS_{PDA} can be effectively blocked by the BN_{PDA} filler network, giving the low electrical conductivity of 1.8×10^{-10} $S \cdot cm^{-1}$. Meanwhile, the $BC/BN_{PDA}/GNS_{PDA}$ composite films effectively transfer the heat and diminish the hot-spot temperature in cooling LED chip module application. Thus, the present study may pave the way to promoting the industrialization of scalable thermal management devices.

Keywords: anisotropic thermal conductivity; electrical insulation; hybrid filler; large-scale; dopamine

Citation: Li, S.; Shen, Y.; Jia, X.; Xu, M.; Zong, R.; Liu, G.; Liu, B.; Huai, X. Dopamine-Mediated Graphene Bridging Hexagonal Boron Nitride for Large-Scale Composite Films with Enhanced Thermal Conductivity and Electrical Insulation. *Nanomaterials* **2023**, *13*, 1210. https://doi.org/10.3390/nano13071210

Academic Editor: Ana M. Benito

Received: 19 February 2023
Revised: 12 March 2023
Accepted: 15 March 2023
Published: 29 March 2023

1. Introduction

More and more attention has been given to the fact that heat accumulation generated in a confined space poses a threat to the service reliability and lifetime of electronic components, especially for the integration and densification of electronic and electrical devices [1–4]. To quickly transfer the excess heat from electrical and electronic devices, it is required to enhance the heat dissipation in a specific direction [5–8]. At the same time, electrical insulation is a prerequisite to ensure the stable and secure operation of thermal management materials in the electric power field [9,10].

Hexagonal boron nitride (BN) possesses excellent dielectric breakdown strength (35 $kV \cdot mm^{-1}$) and high thermal conductivity (180 $W \cdot m^{-1} \cdot K^{-1}$) [11], which is an ideal

filler for the fabrication of the highly thermal conductive and electrical insulation composite materials. For example, BN has been used for embedding into the polymer matrix (comprising natural rubber [12], epoxy resin [13], and cellulose nanofibers [14]) to fabricate functional composite films [15]. However, the existence of interfacial thermal resistance (R_I) significantly affects the heat transfer efficiency along BN filler pathways, for example, the interfaces between BN fillers or between filler and matrix. Thus, many studies have pointed out that the R_I can be reduced by enhancing the interface compatibility through an interface modification strategy [16,17]. In fact, the improvement extent of thermal conductivity also has certain limitations only when reducing the interfacial thermal resistance. This is because the thermal contact resistance (R_c) caused by the poor contact between fillers is another key parameter that determines the final thermal conductivity of composites. It is reported that the contact probability can be effectively increased by introducing another additional filler instead of using only one filler component [18,19]. For instance, the zero-dimensional silver nanoparticles and one-dimensional silicon carbide nanowires were selected to connect BN fillers [20,21]. Compared with the "point-to-point" contact type of zero/one-dimensional materials, two-dimensional materials provide the "face-to-face" contact sites between the thermal conductive fillers [22], which seem to be a very effective strategy for improving effective contact and building a bridge of fillers.

As the most potential two-dimensional material in the thermal management field, graphene nanosheets (GNS) have exceptional thermal conductivity (600–5000 $W \cdot m^{-1} \cdot K^{-1}$) and tensile strength (130 GPa) [23]. Nevertheless, this kind of ultra-high electrical conductivity (10^6 $S \cdot m^{-1}$) makes it hard to directly apply it to the thermal management devices of electronics and the power industry which require good electrical insulation [24]. So, GNS can be used as a candidate for other, supplementary, materials of the main BN filler in order to exploit hybrid composites with excellent thermal conductivity and dielectric properties. However, it is difficult to uniformly disperse two heterogeneous fillers due to the poor interface compatibility, resulting in numerous agglomeration and serious phase separation problems. Moreover, even the most extensive methods of preparing composites, such as hot pressing, vacuum filtration, and freeze-drying, are still far from the industrialized production of scalable and highly arranged composites [25–27]. Therefore, it is highly desirable for the fabrication of large-scale and regularly oriented hybrid composite materials with excellent insulation and thermal conductivity through a convenient and facile approach.

Here, we put forward the dopamine-mediated graphene bridging of hexagonal boron nitride to fabricate the large-scale composite films with enhanced thermal conductivity and electrical insulation. As depicted in Scheme 1, as a biodegradable and naturally recyclable material, dopamine (DA) could easily self-polymerize into polydopamine (PDA) and adhere to the surface of BN and GNS fillers. As another degradable biopolymer, bacterial cellulose (BC), with numerous hydroxyl groups was expected to connect PDA modified hybrid BN and GNS fillers via multiple noncovalent interactions. Finally, the large-scale BC/BN_{PDA}/GNS_{PDA} composite films were prepared through a layer-by-layer (LBL) scraping method. The results demonstrate that the flat and highly directional microstructure of BC/BN_{PDA}/G_{PDA} composite films were successfully built, and the high anisotropic thermal conductivity, enhanced tensile strength, and excellent electrical insulation performances can be effectively balanced by regulating the critical value of the mass ratio of GNS_{PDA} fillers. It was found that the main BN_{PDA} fillers can be bridged by flexible GNS_{PDA} filler to build a continuous and highly oriented thermally conductive pathway under the optimal mass ratio of GNS_{PDA} of 5 wt%; meanwhile, the electrical conductivity arising from GNS_{PDA} can also be effectively blocked by the electrical insulation of h-BN filler. Furthermore, the BC/BN_{PDA}/GNS_{PDA} films show high efficiency in transferring the hot-spot heat from the LED chip, demonstrating great potential applications as thermal management electronic devices.

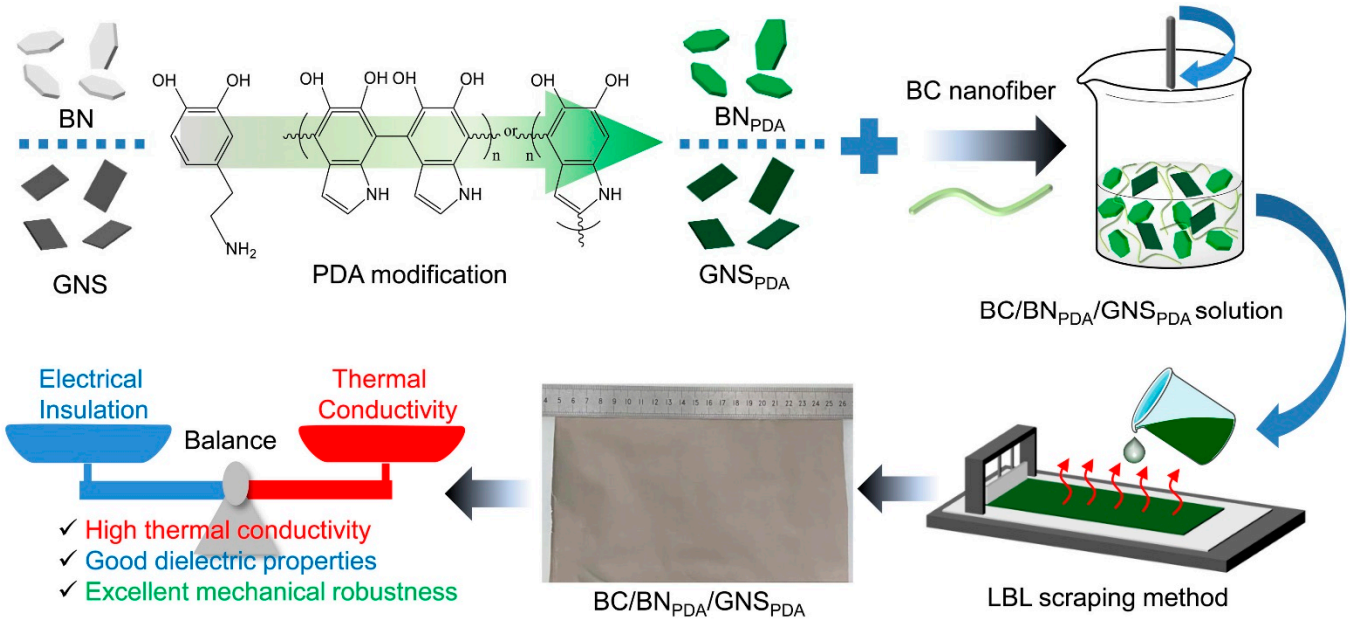

Scheme 1. Schematic illustration of design strategy. Construction of the large-scale $BC/BN_{PDA}/GNS_{PDA}$ composite films from BC nanofibers, PDA-modified BN, and GNS through the LBL scraping method. The highly oriented composite films exhibit enhanced thermal and insulating performance, as well as excellent mechanical robustness.

2. Experimental Section

2.1. Materials

BN (99%, diameter ~7 μm) was purchased from Macklin Biochemical Co., Ltd. (Shanghai, China), and GNS (97%, diameter ~7 μm) was purchased from Kanao Graphene Technology Co., Ltd. (Shenzhen, China). BC (0.73 wt%) was purchased from Qihong Technology Co., Ltd. (Guilin, China). Dopamine (98%), tris(hydroxymethyl)-aminomethane hydrochloride (Tris-HCl) and ethanol were purchased from Beijing Chemical Reagent Co., Ltd. (Beijing, China).

2.2. Preparation of Composite Films

A total of 3 g BN (or GNS) filler and 1.2 g dopamine were added into 500 mL Tris-HCl buffer solution (pH = 8.5). After stirring at room temperature for 24 h, the mixture was filtered and washed with ethanol three times, and the PDA modified BN and GNS fillers were represented as BN_{PDA} and GNS_{PDA}, respectively. Then, the BN_{PDA} and GNS_{PDA} fillers were obtained after drying for 12 h at 60 °C, and the desired content ratio of BN_{PDA} and GNS_{PDA} fillers were added into BC solution (2 mg/mL) and stirred for 3 min. Subsequently, the mixture was cast onto nylon film and heated at 100 °C for 5 min. Finally, the large-scale films were obtained using the layer-by-layer (LBL) scraping method. The composite films composed of BC and hybrid fillers were represented as $BC/BN_{PDA}/GNS_{PDA}$-*X*, and *X* is the mass content of GNS_{PDA} in the hybrid fillers (*X* = 0, 1, 3, 5, 7, and 10).

2.3. Characterization

The morphologies and energy dispersive X-ray spectrometry (EDS) images of filler, matrix and composite films were characterized by emission scanning electron microscopy (SEM, Hitachi, S-4800, Shimadzu, Tokyo, Japan). The Raman spectroscopy of DA, BN, BN_{PDA}, GNS, and GNS_{PDA} fillers was performed on a Raman spectroscope (inVia Reflex, Renishaw, London, UK) with a 532 nm laser excitation wavelength. The thermal degradations of BN, BN_{PDA}, GNS, and GNS_{PDA} fillers were tested by thermogravimetry (TGA, INNUO TGA-1000, Yingnuo, Shanghai, China) under a nitrogen atmosphere (10 °C·min^{-1}, 50–800 °C). X-ray photoelectron spectra (XPS) recorded the chemical composition of BN, BN_{PDA}, GNS, and GNS_{PDA} fillers on an ESCA instrument (Physical Electronics, MA, USA).

Isothermal titration calorimetry (ITC) experiments were performed with a Microcal VP-ITC apparatus at 298.15 K. An X-ray diffractometer (XRD, Rigaku SmartLab 9 kW, Japan) analyzed the orientation of hybrid fillers with a diffraction angle in the range of 2–90°. The mechanical properties of the composite films were tested using a tensile testing machine (AI-7000-LAU10, Gotech Testing Machines Co., Ltd., Dongguan, China). Dielectric properties and the AC conductivity were acquired by the Tong Hui TH26077 Precision LCR Meter in the frequency range of 1000 Hz to 10 MHz. Thermal images were recorded by an infrared camera (Ti400, Fluke, Everett, WA, USA). The numerical simulation software (ANSYS, 16.0) was employed to simulate the heat transfer characteristics of composite films. The anisotropic thermal conductivities of composite films were calculated by the equation: $k = \alpha \times \rho \times C$, where α, ρ, and C, respectively, correspond to the thermal diffusivity, density, and specific heat capacity of composite films, which is measured by the laser flashing method (LFA 467, NanoFlash, Netzch, Germany). C was determined through the following equation: $C = C_{BN} \times \omega + C_{BC} \times (1 - \omega)$, where ω is the filler content and C_{BN} and C_{BC} were separately measured by a differential scanning calorimeter (NETZSCH DSC214, Germany).

3. Results and Discussion

3.1. Characterizations of PDA Modified BN, GNS, and Composite Films

The microstructures and size distributions of BN and GNS fillers are shown in Figure S1a–c. It can be observed that the BN and GNS fillers have a similar filler size (~7 μm), and the GNS filler shows obvious flexibility compared with the brittle BN filler. Meanwhile, Figure S1d displays the SEM images of BC nanofibers, and the inset shows an optical photo of BC solution. It can be seen that the BC nanofibers exhibit a particular ultrafine network structure. The Raman spectra of the DA exhibits the obvious characteristic peak of hydroxyl and amino groups appear separately at 1286 and 1616 cm^{-1} (Figure S2) [28]. Figure 1a displays Raman spectra of the original BN, and GNS fillers and modified BN_{PDA} and GNS_{PDA} fillers. The characteristic peak of BN filler appears at 1364 cm^{-1} [10]. After the PDA modification, a new absorption peak appears near 1557 cm^{-1}, which is attributed to the hydroxyl groups arising from PDA layer on the surface of the BN filler [22]. The Raman shifts at 1263 (weak D-band) and 1575 cm^{-1} (strong G-band) are the characteristic peaks of GNS [24]. After the introduction of PDA, the D-band peak shifts to 1266 cm^{-1} while the G-band peak decreases to 1564 cm^{-1}, which is attributed to the deformation of the catechol groups of the PDA [6]. Figure 1b shows the TGA curves of BN and GNS before and after PDA modification, and BN has no thermal weight loss in the temperature range of 50 to 800 °C, whereas the BN_{PDA} shows thermal degradation between 300 and 650 °C and weight loss reaches 1.89 wt% at 800 °C [5]. GNS and GNS_{PDA} both exhibit obvious thermal degradation, but GNS_{PDA} has a greater weight loss of 3.68 wt% due to the PDA-coated layer. Figure 1c presents the XPS spectra of PDA modified fillers. Compared with the untreated BN filler, the peak intensities of the O and C elements increase but the B and N elements are diminished [5]. For GNS_{PDA}, the N element appears relative to the untreated GNS. In addition, ITC was employed to investigate the thermodynamic behavior of the interactions between BN (or GNS) and PDA (Figure 1d) [5,29]. When the PDA solution was titrated into the BN (or GNS) solution, the observed enthalpy changes (ΔH_{obs}) are negative, indicating that the combination of PDA and BN (or GNS) is accompanied by exothermic process. The ΔH_{obs} value gradually decreases to zero plateau with the addition of PDA solution, which manifests the saturation of the noncovalent binding between PDA and BN or (GNS). The binding constants (K_d) of PDA with BN or GNS can be derived by fitting the ITC curves, and the resulting K_d values give 1.14×10^3 and 3.53×10^3 M^{-1}, respectively, which demonstrates that PDA and BN (or GNS) are effectively combined, and these two fillers have a comparable binding ability with PDA. In brief, this evidence proves that BN and GNS fillers are successfully modified by PDA.

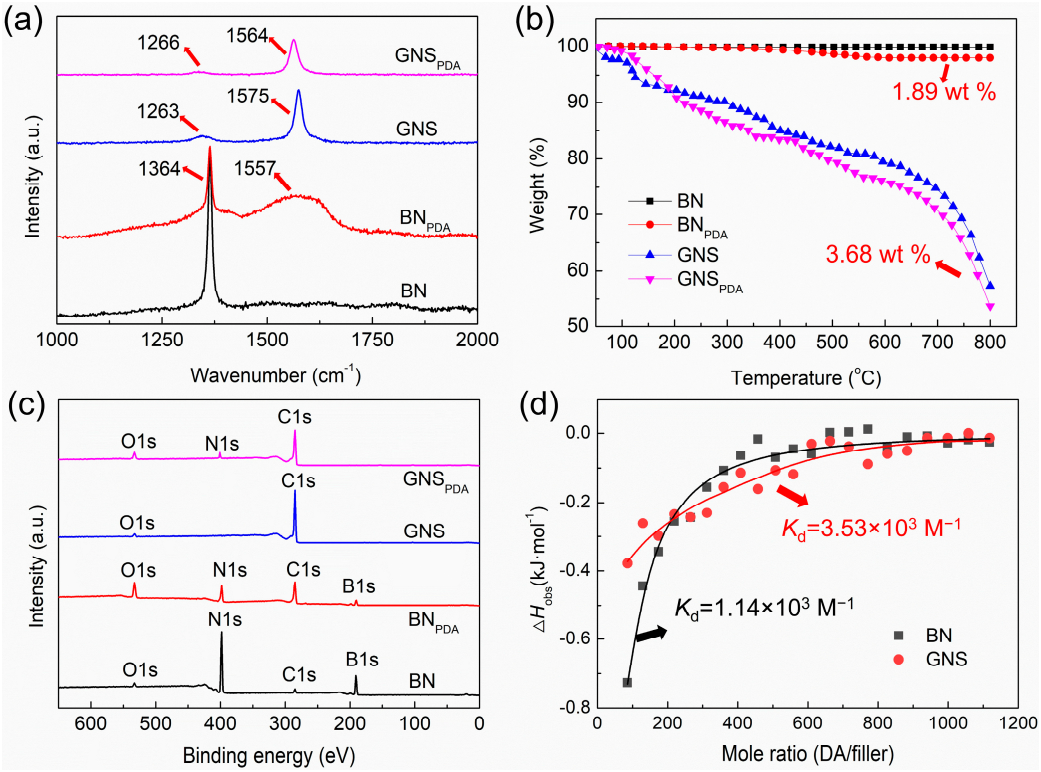

Figure 1. (**a**) Raman spectra, (**b**) TGA analysis, and (**c**) XPS spectra of BN, BN_{PDA}, GNS, and GNS_{PDA}. (**d**) ITC analysis of the enthalpy changes (ΔH_{obs}) relative to the PDA/BN (or GNS) molar ratio.

The cross-section of four films, pure BC (Figure S3), BC/BN_{PDA} (the mass ratio of BN fillers is 70 wt%), BC/BN_{PDA}/GNS_{PDA}-5 (the total mass ratio of hybrid fillers is 70 wt% and the mass ratio of GNS_{PDA} is 5 wt%), and BC/BN_{PDA}/GNS_{PDA}-10 (the total mass ratio of hybrid fillers is 70 wt% and the mass ratio of GNS_{PDA} is 10 wt%) were observed from SEM. Figure 2a presents the cross-sectional morphology of the BC/BN_{PDA} film, which shows the partially oriented stacking of BN_{PDA} fillers (as revealed by the red arrows) [5]. After the introduction of 5 wt% GNS_{PDA}, the cross-section of BC/BN_{PDA}/GNS_{PDA}-5 film exhibits more regular arrangement and forms longer networks of hybrid fillers relative to BC/BN_{PDA} film, as shown in Figure 2b. This may be because GNS_{PDA} plays a key role in face-to-face contact with the BN_{PDA} filler, making the formation a continuous network structure inside the BC/BN_{PDA}/GNS_{PDA}-5 film. Simultaneously, the energy dispersive spectrometer (EDS) mapping of the BC/BN_{PDA}/GNS_{PDA}-5 film (Figure 2d) clearly shows the lamellar distributions of B, N, and C elements, which confirms the well-stacked layered structure of the hybrid fillers. Moreover, when the mass ratio of GNS_{PDA} increases to 10 wt%, the uniform and close networks of BC/BN_{PDA}/GNS_{PDA}-10 film appear in Figure 2c. Additionally, this result indicates that the probability of effective contact between hybrid fillers significantly increases, which is beneficial for forming a denser and complete "BN-GNS-BN" pathway.

To further to evaluate the orientations of BN fillers, XRD measurements on BC/BN_{PDA} and BC/BN_{PDA}/GNS_{PDA}-5 were performed. As shown in Figure 2e, two characteristic peaks arising from BC nanofiber appear at 15° and 23°. Moreover, the characteristic peaks at 27° and 42° arise from the (002) and (100) planes of the BN fillers, and the intensities of these two peaks are expressed as I_{002} and I_{100}. It is reported that the increased values of I_{002}/I_{100} means the improved in-plane orientation of BN fillers for the composite film [20]. Take the example of the BC/BN_{PDA}/GNS_{PDA}-5 film: the I_{002}/I_{100} value of BC/BN_{PDA}/GNS_{PDA}-5 film gives 132, which is obviously higher than that of BC/BN_{PDA} films (89) [5]. Thus, by the aid of the flexible GNS_{PDA}, the orientation of BN fillers along the in-plane direction is greatly enhanced. This result is consistent with the observed morphology features,

which shows that the BC/BN_{PDA}/GNS_{PDA} film exhibits increased in-plane interconnected structures relative to BC/BN_{PDA} films. In general, the distribution of GNS_{PDA} in the hybrid fillers is closely related to the formation of thermal contact channels in composite films, which directly determines the heat transfer efficiency. As illustrated in Figure 2f–h, the BC/BN_{PDA} film shows randomly oriented BN networks. After the introduction of GNS_{PDA} filler, the BN_{PDA} fillers can be connected by GNS_{PDA} fillers to form the more continuous and longer "BN-GNS-BN" pathways (Figure 2g,h), which are beneficial for filling the interfacial gap between BN and BC and improving the insufficient contact between the brittle BN fillers. Therefore, by introducing a small amount of GNS_{PDA} filler, the interface compatibility between hybrid fillers and BC matrix is improved, and more importantly, the possibility of effective contact between hybrid fillers is also enhanced, which is expected to diminish the heat transfer resistance in the interfacial thermal resistance (R_I) and thermal contact resistance (R_c).

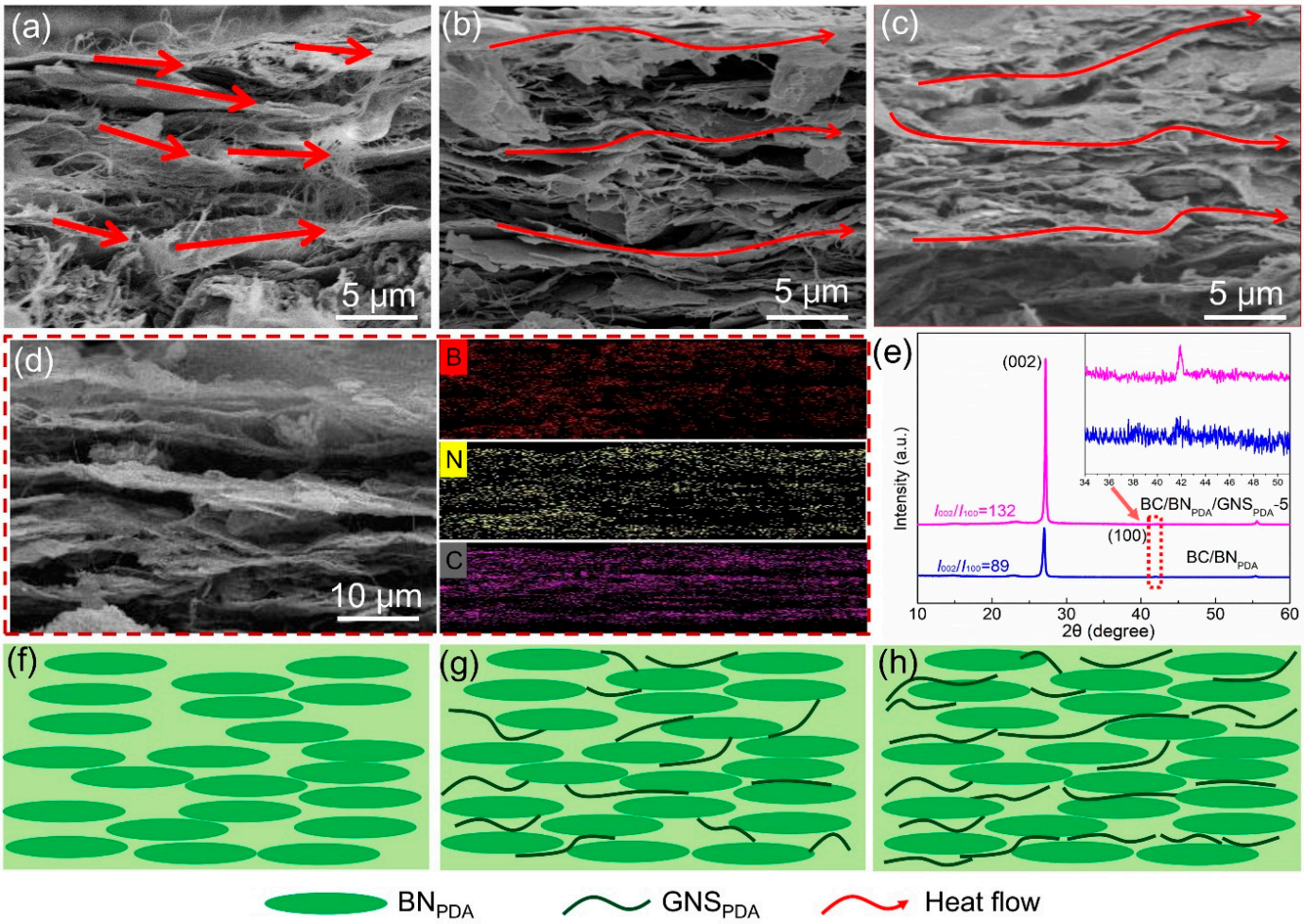

Figure 2. (**a**–**c**) SEM images of cross section of three composite films: BC/BN_{PDA}, BC/BN_{PDA}/GNS_{PDA}-5, and BC/BN_{PDA}/GNS_{PDA}-10. (**d**) Elemental mapping images of B, N, and C in the BC/BN_{PDA}/GNS_{PDA}-5 composite film. (**e**) XRD patterns of BC/BN_{PDA} and BC/BN_{PDA}/GNS_{PDA}-5 composite films. (**f**–**h**) Schematic diagrams of the distributions of hybrid fillers.

3.2. Thermal Conductivity of Composite Films

The continuous and regularly oriented heat conduction pathway is the core of heat transfer process. The anisotropic thermal conductivities of different composite films at varied hybrid fillers contents were measured through the LFA method (details described in S1 in the Supplementary Materials). In our previous work, the thermal conductivity of BC/BN_{PDA} films obtained by vacuum filtration are 21.6 $W \cdot m^{-1} \cdot K^{-1}$ [5], and these

values are close to the results of BC/BN_{PDA} films prepared using the LBL scraping method (21.7 $W \cdot m^{-1} \cdot K^{-1}$). Figure 3a shows that the BC/BN_{PDA}/GNS_{PDA}-5 composite films always exhibit higher in-plane thermal conductivities than BC/BN_{PDA} films at varied filler contents. In particular, the in-plane thermal conductivity of the BC/BN_{PDA}/GNS_{PDA}-5 composite film reaches 34.9 $W \cdot m^{-1} \cdot K^{-1}$ at the hybrid filler mass ratio of 70 wt%, which increases to 161% relative to the BC/BN_{PDA} film (21.7 $W \cdot m^{-1} \cdot K^{-1}$) [5]. By contrast, Figure 3b displays the through-plane thermal conductivities of the BC/BN_{PDA}/GNS_{PDA}-5 composite films, which are of lower values than those of BC/BN_{PDA} films at different filler contents. This may be because the introduction of a small amount of GNS_{PDA} (5 wt%) plays an important role in bridging the main BN filler (95 wt%), which greatly increases the contact of BN fillers along the in-plane direction, as observed from the continuous and well-stacked BN structure in Figure 2b, which is conducive to enhancing the anisotropic heat transfer efficiency of BC/BN_{PDA}/GNS_{PDA}-5 composite films. The effect of GNS_{PDA} contents on the in-plane thermal conductivities of the BC/BN_{PDA}/GNS_{PDA} films (the total content of hybrid fillers is fixed at 70 wt%) is also considered. Since the high content of GNS will lead to poor electrical insulation performance [6], the influence of GNS_{PDA} contents in the range of 0~10 wt% on the in-plane thermal conductivity is investigated in Figure 3c. It can be clearly observed that the in-plane thermal conductivity of the composite film has a significant increase when the mass ratio of GNS_{PDA} reaches 5 wt%, but the improvement extent of in-plane thermal conductivities is limited by further increasing the mass ratio of GNS_{PDA}. Therefore, the synergistic effect between GNS_{PDA} and BN_{PDA} may exist in improving heat transfer efficiency at the critical GNS_{PDA} content of 5 wt%.

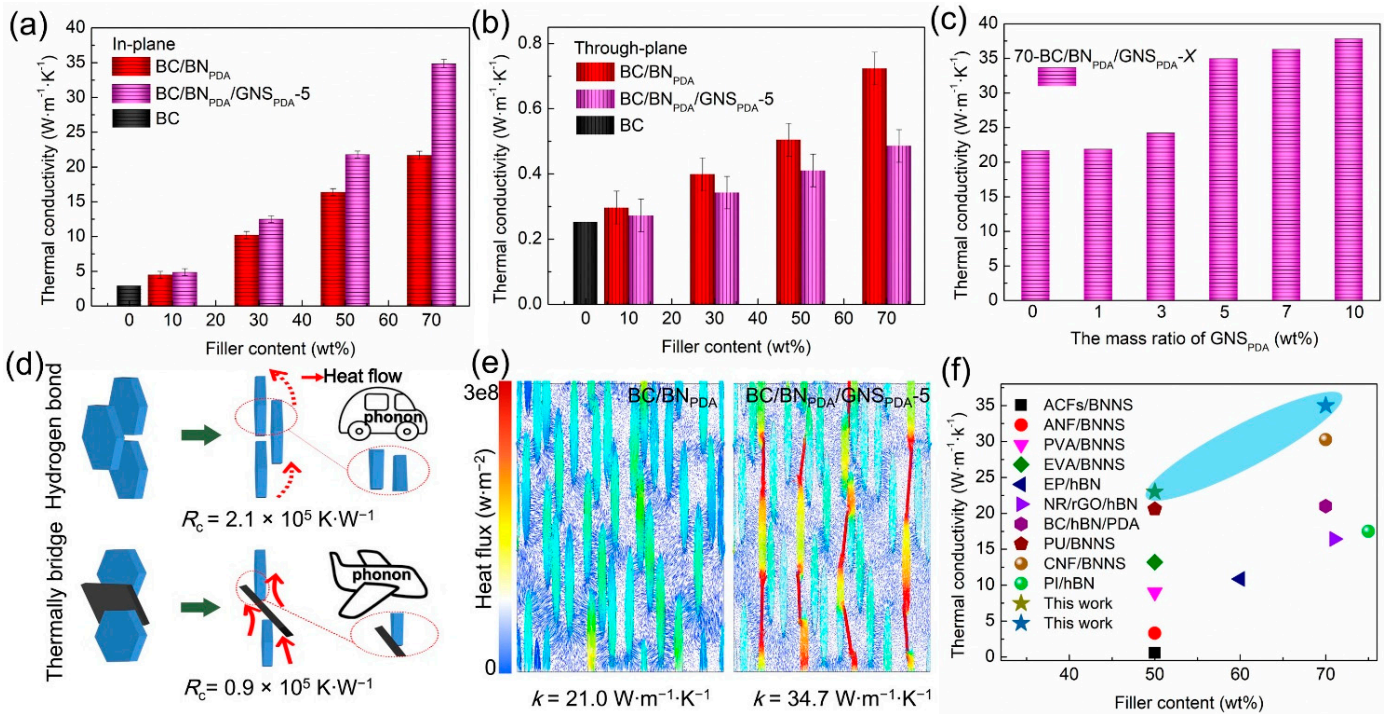

Figure 3. (**a**) In-plane and (**b**) through-plane thermal conductivities of two composite films: BC/BN_{PDA} and BC/BN_{PDA}/GNS_{PDA}-5 at different filler contents. (**c**) In-plane thermal conductivities of the 70 wt% BC/BN_{PDA}/GNS_{PDA} composite films at different mass ratios of GNS_{PDA}. (**d**) Schematic diagram of the effect of contact thermal resistance on phonon transport. (**e**) Numerical simulation of heat transfer behaviors between BC/BN_{PDA} and BC/BN_{PDA}/GNS_{PDA}-5 films in the preferred direction. (**f**) Comparisons of in-plane thermal conductivity of this work with the reported BN-based composites from the literature.

It Is essential to elucidate the effect of a small mass ratio of GNS_{PDA} (5 wt%) on the thermal conductivity of the composite films, and thus, the effective medium theory (EMT) [25] and Foygel model [10] were used to investigate their influence on interfacial thermal resistance (R_I) and thermal contact resistance (R_c) of inner composite films. According to the in-plane thermal conductivity of the composite films, the EMT model is employed to calculate the R_I values between filler and BC matrix before and after the introduction of GNS_{PDA}, and the corresponding equations are shown below:

$$k = k_m \frac{3 + f\left(\beta_\perp + \beta_\parallel\right)}{3 - f\beta_\perp} \tag{1}$$

$$\beta_\perp = \frac{2\left(d\left(k_f - k_p\right) - 2R_I k_f k_p\right)}{d\left(k_f + k_p\right) + 2R_I k_f k_p} \tag{2}$$

$$\beta_\parallel = \frac{L\left(k_f - k_p\right) - 2R_I k_f k_p}{Lk_p + 2R_I k_f k_p} \tag{3}$$

where k_p (3.05 $W{\cdot}m^{-1}{\cdot}K^{-1}$, Table S1), k_f (180 $W{\cdot}m^{-1}{\cdot}K^{-1}$), and k are the in-plane thermal conductivities of BC matrix, BN fillers, and composite films, respectively; f is the volume fraction of filler; d (0.5 μm) and L (7.0 μm) are the thickness and lateral size of BN (Figure S1); and R_I is obtained by using the EMT equations (Figure S2). The resulting R_I of BC and BN_{PDA}/GNS_{PDA}-5 gives 1.83×10^{-8} $m^2{\cdot}K{\cdot}W^{-1}$, which is evidently lower than the BC and BN_{PDA} (3.06×10^{-8} $m^2{\cdot}K{\cdot}W^{-1}$). These results demonstrate that a small amount of GNS_{PDA} (5 wt%) eliminates interfacial gaps, thereby reducing the interfacial thermal resistance between the filler and the BC matrix.

The Foygel model was further employed to clarify the introduction of flexible GNS_{PDA} filler on the R_c of composite films, which can be described as follows (calculated details in S2 in the Supplementary Materials):

$$k - k_p = k_0 \left[\frac{f - f_c}{1 - f_c}\right]^\tau \tag{4}$$

$$R_c = \frac{1}{k_0 L {f_c}^\tau} \tag{5}$$

where k_0 is a pre-exponential factor ratio determined by the interconnected BN networks; f_c is the measured and critical volume fraction of the hybrid fillers in the films; and τ is the conductivity exponent determined by the aspect ratio of the BN. The f_c, k_0, and τ values are 15 vol%, 44, and 0.62 for $BC/BN_{PDA}/GNS_{PDA}$-5 and 10 vol%, 28, and 0.56 for BC/BN_{PDA}, respectively, and R_c is obtained by combing the above Foygel model equations. As a result, the R_c between partially connected "BN-GNS-BN" interfaces is calculated to be 0.9×10^5 $K{\cdot}W^{-1}$, which is approximately half of that of "BN-BN" interfaces (2.1×10^5 $K{\cdot}W^{-1}$), which demonstrates more contact probability of filler and efficient phonon transport in $BC/BN_{PDA}/GNS_{PDA}$-5 films (Figure 3d).

The heat transfer distributions of composite films in the presence and absent of GNS_{PDA} filler is simulated using the finite element, and finite element models, boundary conditions, and mesh distributions were detailed described in S3 in the Supplementary Materials. Figure 3e displays the calculated heat flux distributions and thermal conductivities of BC/BN_{PDA} and $BC/BN_{PDA}/GNS_{PDA}$-5 composite films. For BC/BN_{PDA} film, the BN fillers exhibit obvious randomly oriented distributions, and the heat flux vector is mainly distributed along the BN pathway. Meanwhile, the noncontact BN fillers contain numerous BN–BN interfaces, and large thermal scattering remains at the edges of h-BN fillers. By contrast, for $BC/BN_{PDA}/GNS_{PDA}$-5 film, the higher heat flux vector is mainly distributed along the "BN-GNS-BN" pathway due to the adjacent BN_{PDA} fillers are bridged by flexible GNS_{PDA}. Additionally, the relative longer and denser thermally conductive pathways along hybrid fillers are formed, which effectively minimizes the phonon interface scattering. The numerical thermal conductivities of BC/BN_{PDA} and $BC/BN_{PDA}/GNS_{PDA}$-5 composite films are separately 21.0 and 34.7 $W{\cdot}m^{-1}{\cdot}K^{-1}$, which

are approximately consistent with the experimental values (21.7 and 34.9 $W \cdot m^{-1} \cdot K^{-1}$) at the fixed filler content of 70 wt% (Figure 3a). Furthermore, Figure 3f further compares the thermal conductivities of $BC/BN_{PDA}/GNS_{PDA}$-5 composite films in this work with BN-based fillers composites from the literature at the fixed filler content [5,19,30–37], which suggests that the $BC/BN_{PDA}/GNS_{PDA}$-5 films prepared using present strategy show satisfactory in-plane thermal conductivity.

Given that GNS can bridge BN to extend the "BN" pathway, the aspect ratio of BN fillers should be carefully considered to further improve the performance of the composites. This is because many studies pointed out that the increment of filler aspect ratio will significantly improve the phonon mean free path and the thermal conductive pathway [10], and our recent research also reveals that the thermal conductivity of composites can increase to 330% when the aspect ratio of BN increases from 5 to 25 [8]. However, the most available methods for the preparation of high aspect ratio BN fillers, including ultrasonic, ball milling, and liquid-phase exfoliation methods, generally involve the problems of complex synthesis, cumbersome process steps, and low yields. The challenges in obtaining scalable high aspect ratio of BN fillers makes it hard to directly apply our developed strategy to the industrialized production of composites. Thus, it would be of great interest to further investigate the effect of ultrahigh aspect ratio BN filler on the mechanical, electrical, and thermal properties in the future works.

3.3. Mechanical and Dielectric Properties of Composite Films

In addition to the highly anisotropic thermal conductivity of composite films, the good mechanical and electrical insulation is also of great significance for practical applications. Figure 4a,b reveal the tensile strength and elongation at break of the BC/BN_{PDA} and the $BC/BN_{PDA}/GNS_{PDA}$-5 composite films at varied filler contents. It can be seen that the pure BC film shows good mechanical strength (66.1 MPa), which is similar to the results found in the literature [5,38]. Evidently, the $BC/BN_{PDA}/GNS_{PDA}$-5 films exhibit higher tensile strength and elongation at break relative to BC/BN_{PDA} films. For example, the tensile strength of the $BC/BN_{PDA}/GNS_{PDA}$-5 film is 30.9 MPa at 70 wt% filler content, which increases to 156% relative to BC/BN_{PDA} film (19.8 MPa). At the same time, the elongation at break of $BC/BN_{PDA}/GNS_{PDA}$-5 film reaches 4.1%, which increases to 205% compared with BC/BN_{PDA} film (2.0%). This can be analyzed through the microstructures in SEM images. On the basis of the "nacre-like" lamellar structures of BC/BN_{PDA} films, there are few interfacial gaps between BN_{PDA} and BC nanofibers (Figure 2a), which destroy the formation of continuous and complete the BC nanofiber networks. With the introduction of PDA-modified GNS filler, the GNS_{PDA} has a better match with BC matrix in intrinsic flexibility and can be completely covered by the BC nanofibers and BN_{PDA} fillers (Figure 2b), thus forming a more continuous network structure within the film. Therefore, the GNS_{PDA} filler can play a flexible bridge role in connecting isolated and brittle BN fillers, thus effectively transferring the stress and delaying the deformation of the composite film. In addition, we also performed the stress−strain experiments on the $BC/BN_{PDA}/GNS_{PDA}$-5 composite films at varied filler contents, as presented in Figure S8a. The ultimate tensile strength and elongation at break at different filler contents are basically consistent with the experimental results in Figure 4a,b. For example, at the fixed filler content of 70 wt%, the ultimate tensile strength and elongation at break are 29.7 MPa and 4.0%, respectively, which are basically consistent with results from Figure 4a,b (30.9 MPa and 4.1%). Figure S8b shows that the $BC/BN_{PDA}/GNS_{PDA}$-5 composite films at the hybrid filler content of 70 wt% can easily lift a 500 g weight, indicating the robust mechanical property [39,40]. Figure 5c presents the tensile recovery result of the $BC/BN_{PDA}/GNS_{PDA}$-5 film at the fixed filler content of 70 wt%, and it was found that when the tensile strain of the film gradually increases from 1.5 to 4%, the stress of the film at 1.5% strain is 3.0, 4.3, 6.5, 7.4, and 8.5 MPa, respectively, exhibiting an obvious increasing trend. This is because when the film is stretched, the ultrahigh aspect-ratios of the BN_{PDA}, GNS_{PDA}, and BC matrix will be further distributed along the in-plane orientation, forming a tighter network structure, thus strengthening the mechanical properties.

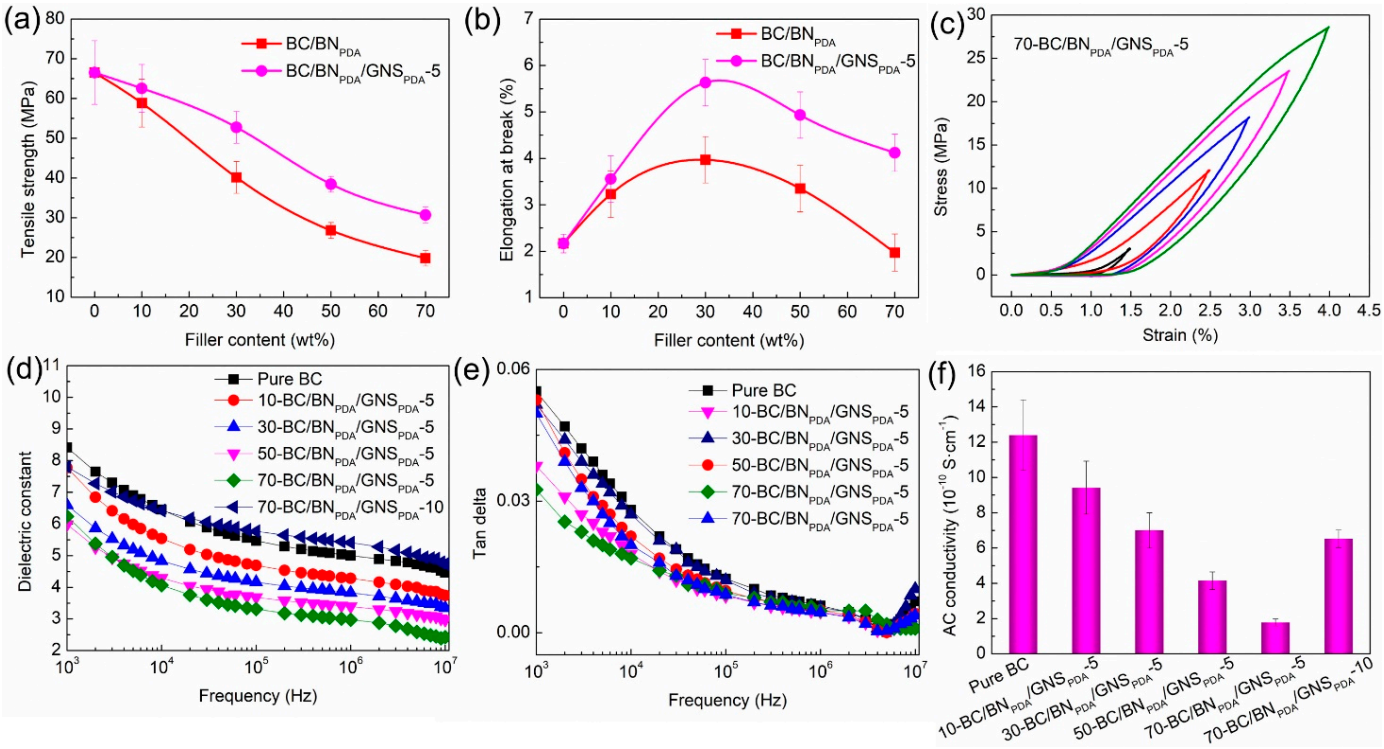

Figure 4. (**a**) Tensile strength and (**b**) elongation at break of the BC/BN$_{PDA}$ and BC/BN$_{PDA}$/GNS$_{PDA}$-5 films with different hybrid fillers contents. (**c**) The tensile recovery curves of the 70 wt% BC/BN$_{PDA}$/GNS$_{PDA}$-5 films. (**d**) Dielectric constant (ε), (**e**) dielectric loss (tanδ), and (**f**) AC conductivity of the BC/BN$_{PDA}$/GNS$_{PDA}$ composite films at varied hybrid fillers contents.

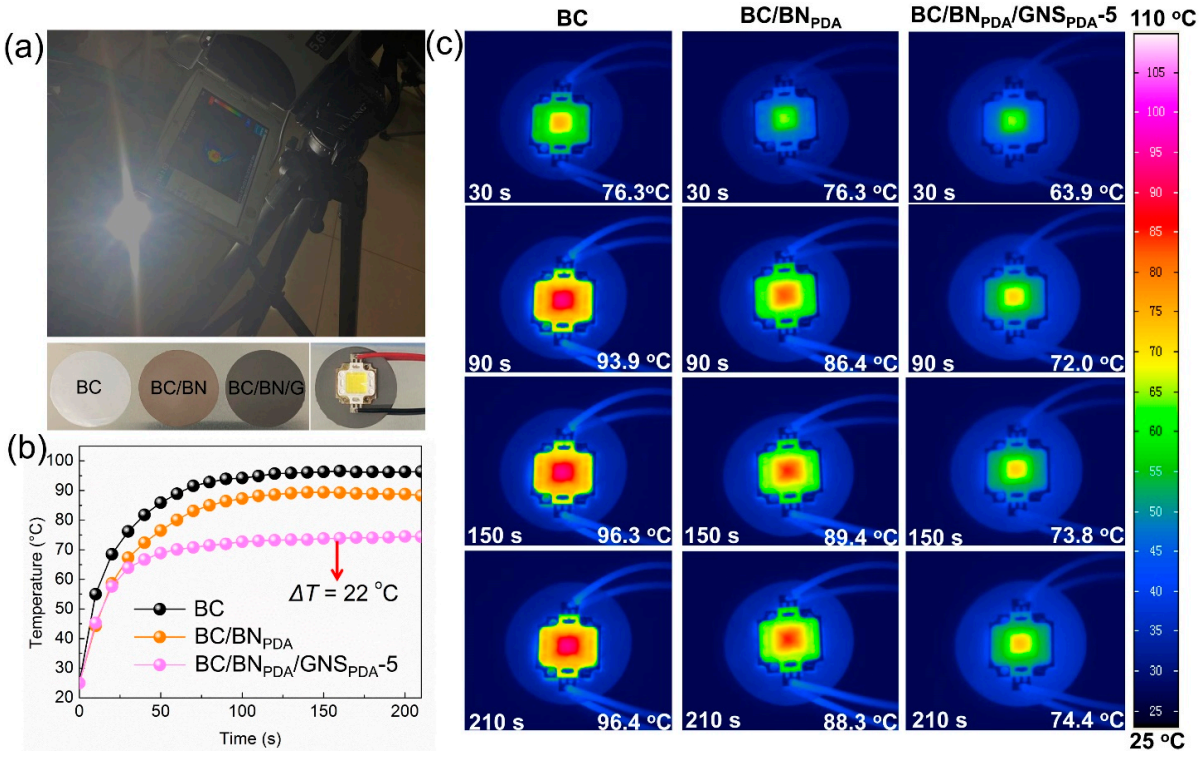

Figure 5. (**a**) Experimental configuration for testing the heat transfer performance of BC, BC/BN$_{PDA}$, and BC/BN$_{PDA}$/GNS$_{PDA}$-5 films applied to LED chip heat dissipation. (**b**) Temperature evolution of LED chip as a function of running time and (**c**) the corresponding IR images of temperature distributions of BC, BC/BN$_{PDA}$, and BC/BN$_{PDA}$/GNS$_{PDA}$-5 films.

The reduction of electron delocalization arising from the ionic characteristic of the B−N bond generally brings about large band gap of the BN filler, which provides the excellent electrical insulating features of composites [41]. Conversely, the conjugated structures of GNS has high electron mobility (2×10^5 $cm^2 \cdot V^{-1} \cdot s^{-1}$) [24], which leads to poor electrical insulation properties. It was found, surprisingly, that the electrical insulation properties can be regulated by controlling the mass ratio of GNS_{PDA}. Figure 4d,e depicts the dielectric constant (ε) and dielectric loss (tanδ) of composite films at varied filler content. It can be seen that the ε and tanδ values of BC/BN_{PDA}/GNS_{PDA}-5 films are clearly reduced with the increase in hybrid fillers contents, which has a similar trend seen in the literature [5,37]. For example, the ε and tanδ values of the BC/BN_{PDA}/GNS_{PDA}-5 composite film with 70 wt% hybrid fillers contents separately reach the extremely low values of 6.3 and 0.03 at the frequency of 1000 Hz, which are lower than that of the film with 10 wt% hybrid fillers (8.1 and 0.05). This is because the BN is the main filler, which exhibits an extremely low values of ε and tanδ (~4, ~5×10^{-4}) [42]; that being said, some studies have reported that the addition of GNS causes the enhancement of ε due to the interfacial polarization effect and the formation of the micro-capacitance [43]. However, for the hybrid filler of the prepared BC/BN_{PDA}/GNS_{PDA}-5 film, the content of GNS filler (5 wt%) is much lower than that of the BN filler (95 wt%), and the small amount of GNS is isolated by numerous BN fillers, so the GNS filler fails to form micro-capacitances inner composites. However, when the mass ratio of GNS_{PDA} increases to 10 wt%, the ε and tanδ values for the BC/BN_{PDA}/GNS_{PDA}-10 film increase to 7.8 and 0.05, which are apparently increased relative to the BC/BN_{PDA}/GNS_{PDA}-5 film. This result shows that when the amount of GNS fillers exceeds the critical value, GNS fillers might connect to each other, resulting in the interfacial polarization effect [44]. Therefore, when the content of GNP is about 5 wt%, it is beneficial to ensure that the composite film exhibits excellent dielectric properties. Moreover, as presented in Figure 4f, at the fixed GNS_{PDA} of 5 wt%, the AC conductivity of BC/BN_{PDA}/GNS_{PDA}-5 film can be dramatically decreased with the increase in the hybrid fillers contents, further showing an obvious enhancement of electrical insulation properties [37]. However, when the mass ratio of GNS_{PDA} further increases to 10 wt %, the AC conductivity of the BC/BN_{PDA}/GNS_{PDA}-10 film further increases to 6.5×10^{-10} $S \cdot cm^{-1}$, which is a significant enhancement compared to the BC/BN_{PDA}/GNS_{PDA}-5 film (1.8×10^{-10} $S \cdot cm^{-1}$). This may be because when the mass ratio of GNS_{PDA} is close to a critical value (5 wt%), the electrical conductivity caused by GNS_{PDA} could be largely cut off by the excellent electrical insulation of h-BN filler networks. As a result, the low dielectric constant, dielectric loss, and electrical conductivity, as well as high thermal conductive properties, can be effectively balanced by simply tuning the mass ratio of the supplementary GNS_{PDA} filler.

3.4. Heat Dissipation Application of the BC/BN_{PDA}/GNS_{PDA}-5 Composite Films

Given the highly thermal conductivity and electrical insulation, as well as excellent mechanical robustness, the BC/BN_{PDA}/GNS_{PDA}-5 composite films have potential applications in the thermal management of cooling high-power electronic devices. Here, the cooling efficiency of three composite films, including pure the BC, BC/BN_{PDA}, and BC/BN_{PDA}/GNS_{PDA}-5 films, is compared through heat dissipation experiments. As displayed in Figure 5a, the LED chip (10 W) was placed in the middle of films, and the aluminum plate was directly mounted on the films to ensure effective heat diffusion. The IR camera was used to record the hot-spot temperature changes and the temperature distributions images of LED chips. As shown in Figure 5b,c, the LED chip achieves a lower temperature of 74.4 °C within 200 s using the BC/BN_{PDA}/GNS_{PDA}-5 films, which is, respectively, 22 °C and 13.9 °C lower than when using the BC (96.4 °C) and BC/BN_{PDA} films (88.3 °C). It is worth noting that the operation temperature of LED chips closely relates to their working lifetimes; for example, it is reported that every 10 °C drop in chip temperature can extend its service life by 50% [5]. Therefore, the BC/BN_{PDA}/GNS_{PDA}-5 film can effectively dissipate the heat and quickly reduce the hot spot temperature, which reveals great potential for use in electronic packaging and electrical thermal management applications.

4. Conclusions

In summary, we developed a facile route to fabricate large-scale composite films using the assembly of PDA-functionalized GNS and BN fillers, as well as BC nanofibers. The introduction of the PDA layer greatly improved the interface compatibility between the GNS filler, BN filler, and BC matrix, and the presence of GNS_{PDA}-bridging significantly increased the probability of effective contact with BN_{PDA} fillers. The reduction in R_I and R_c was conducive to the formation of the well stacked and highly oriented microstructure of the $BC/BN_{PDA}/GNS_{PDA}$ composite film, which was beneficial when forming a denser and complete "BN-GNS-BN" heat conduction pathway and tight filler–matrix network. For example, the $BC/BN_{PDA}/GNS_{PDA}$ composite film shows a thermal conductivity and tensile strength of 34.9 $W \cdot m^{-1} \cdot K^{-1}$ and 30.9 MPa, which separately increased to 161% and 155% relative to the BC/BN_{PDA} film. Although the introduction of the high electric conductivity GNS_{PDA} may affect the electrical insulation of composites, it was found that the low electrically conductive and high thermal conductive properties can be well balanced by regulating the critical value of the mass ratio of GNS_{PDA} fillers. At the optimal GNS_{PDA} mass ratio of 5 wt%, the electrical conductivity caused by GNS_{PDA} could be effectively blocked by the BN_{PDA} filler network, thereby resulting in a low electrical conductivity of 1.8×10^{-10} $S \cdot cm^{-1}$. Moreover, the $BC/BN_{PDA}/GNS_{PDA}$ composite films effectively transfer heat and diminish the hot spot temperature in LED chip cooling applications. The present concise strategy simultaneously meets the high anisotropic thermal conductivity and low electrical conductivity demands, and it may pave the way to promoting the potential of the industrialization of scalable thermal management devices.

Supplementary Materials: The following are available online at https://www.mdpi.com/article/10.3390/nano13071210/s1, Figure S1. (a,b) SEM images and filler size distributions of BN and GNS fillers. (c–f) The measured thicknesses of BN filler, which are composed by white lines and arrows. (g) SEM images of BC nanofibers, and the inset shows optical photo of BC solution. Figure S2. Raman spectra of DA. Figure S3. SEM images of cross-section of pure BC film. Figure S4. The R_I values were calculated by fitting the in-plane thermal conductivities of the BC/BN_{PDA} and $BC/BN_{PDA}/GNS_{PDA}$-5 composite film based on the EMT model. Figure S5. Foygel model fitting curves of BC/BN_{PDA} and $BC/BN_{PDA}/GNS_{PDA}$-5 composite films, respectively. Figure S6. Linear fitting results based on Foygel model for (a) BC/BN_{PDA} and (b) $BC/BN_{PDA}/GNS_{PDA}$-5 composite films. Figure S7. (a,b) The finite element models of the composite films: BC/BN_{PDA} and $BC/BN_{PDA}/GNS_{PDA}$-5. (c,d) The mesh distributions of the composite films: BC/BN_{PDA} and $BC/BN_{PDA}/GNS_{PDA}$-5. Figure S8. (a) Stress−strain curves of $BC/BN_{PDA}/GNS_{PDA}$-5 composite films at varied filler content. (b) The optical image of 70 wt % $BC/BN_{PDA}/GNS_{PDA}$-5 film lifting a 500 g weight. Table S1. The in-plane ($\alpha_{\parallel}$) and through-plane ($\alpha_{\perp}$) thermal diffusivity, density (ρ), and specific heat capacity (C) of composite films at different filler contents. References [45,46] are cited in the Supplementary Materials.

Author Contributions: Conceptualization, methodology, and writing—original draft preparation, S.L.; supervision, Y.S. and B.L.; resources, M.X., G.L. and X.H.; writing—review, Y.S.; funding acquisition, B.L. and X.J.; investigation, R.Z. All authors have read and agreed to the published version of the manuscript.

Funding: This work was supported by the National Natural Science Foundation of China (51606190 and 52006219) and the Strategic Priority Research Program of the Chinese Academy of Sciences ("Transformational Technologies for Clean Energy and Demonstration", Grant No. XDA 21000000).

Data Availability Statement: Data are available upon request from the authors.

Conflicts of Interest: The authors declare no conflict of interest.

References

1. van Erp, R.; Soleimanzadeh, R.; Nela, L.; Kampitsis, G.; Matioli, E. Co-designing electronics with microfluidics for more sustainable cooling. *Nature* **2020**, *585*, 211–216. [CrossRef] [PubMed]
2. Wu, S.; Li, T.; Wu, M.; Xu, J.; Hu, Y.; Chao, J.; Yan, T.; Wang, R. Highly Thermally Conductive and Flexible Phase Change Composites Enabled by Polymer/Graphite Nanoplatelet-Based Dual Networks for Efficient Thermal Management. *J. Mater. Chem. A* **2020**, *8*, 20011–20020. [CrossRef]

3. Liu, Z.; Xu, J.; Xu, M.; Huang, C.; Wang, R.; Li, T.; Huai, X. Ultralow-Temperature-Driven Water-Based Sorption Refrigeration Enabled by Low-Cost Zeolite-Like Porous Aluminophosphate. *Nat. Commun.* **2022**, *13*, 193. [CrossRef]
4. Li, T.; Wu, M.; Wu, S.; Xiang, S.; Xu, J.; Chao, J.; Yang, T.; Deng, T.; Wang, R. Highly Conductive Phase Change Composites Enabled by Vertically-Aligned Reticulated Graphite Nanoplatelets for High-Temperature Solar Photo/Electro-Thermal Energy Conversion, Harvesting and Storage. *Nano Energy* **2021**, *89*, 106388. [CrossRef]
5. Li, S.; Liu, B.; Jia, X.; Xu, M.; Liu, Z.; Liu, G.; Huai, X. Dopamine-Mediated Bacterial Cellulose/Hexagonal Boron Nitride Composite Films with Enhanced Thermal and Mechanical Performance. *Ind. Eng. Chem. Res.* **2022**, *61*, 4601–4611. [CrossRef]
6. Liu, Y.; Wu, K.; Luo, F.; Lu, M.; Xiao, F.; Du, X.; Zhang, S.; Liang, L.; Lu, M. Significantly enhanced thermal conductivity in polyvinyl alcohol composites enabled by dopamine modified graphene nanoplatelets. *Compos. Part A* **2019**, *117*, 134–143. [CrossRef]
7. Sun, H.; Jiang, Y.; Hua, R.; Huang, R.; Shi, L.; Dong, Y.; Liang, S.; Ni, J.; Zhang, C.; Dong, R.; et al. Graphene and 2D Hexagonal Boron Nitride Heterostructure for Thermal Management in Actively Tunable Manner. *Nanomaterials* **2022**, *12*, 4057. [CrossRef]
8. Li, S.; Liu, B.; Jia, X.; Xu, M.; Zong, R.; Li, X.; Liu, G.; Huai, X. Numerical Simulation on the Optimization of the Anisotropic Thermal Conductivity of Hexagonal Boron Nitride/Nanofiber Composite Films. *Ind. Eng. Chem. Res.* **2023**, *62*, 3183–3193. [CrossRef]
9. Liang, C.; Ruan, K.; Zhang, Y.; Gu, J. Multifunctional Flexible Electromagnetic Interference Shielding AgNWs/Cellulose Films with Excellent Thermal Management and Joule Heating Performances. *ACS Appl. Mater. Interfaces* **2020**, *12*, 18023–18031. [CrossRef]
10. Yan, Q.; Dai, W.; Gao, J.; Tan, X.; Lv, L.; Ying, J.; Lu, X.; Lu, J.; Yao, Y.; Wei, Q.; et al. Ultrahigh-Aspect-Ratio Boron Nitride Nanosheets Leading to Superhigh In-Plane Thermal Conductivity of Foldable Heat Spreader. *ACS Nano* **2021**, *15*, 6489–6498. [CrossRef]
11. Kim, K.; Hsu, A.; Jia, X.; Kim, S.; Tomas, P.; Kong, J. Synthesis and Characterization of Hexagonal Boron Nitride Film as a Dielectric Layer for Graphene Devices. *ACS Nano* **2012**, *6*, 8583–85903. [CrossRef] [PubMed]
12. Hu, Q.; Bai, X.; Zhang, C.; Zeng, X.; Huang, Z.; Li, J.; Li, J.; Zhang, Y. Oriented BN/Silicone rubber composite thermal interface materials with high out-of-plane thermal conductivity and flexibility. *Compos. Part A* **2022**, *152*, 106681. [CrossRef]
13. Li, M.; Wang, M.; Hou, X.; Zhan, Z.; Wang, H.; Fu, H.; Lin, C.; Fu, L.; Jiang, N.; Yu, J. Highly thermal conductive and electrical insulating polymer composites with boron nitride. *Compos. B Eng.* **2020**, *184*, 107746. [CrossRef]
14. Zhang, F.; Lian, M.; Alhadhrami, A.; Huang, M.; Li, B.; Mersal, G.; Ibrahim, M.; Xu, M. Laccase immobilized on functionalized cellulose nanofiber/alginate composite hydrogel for efficient bisphenol A degradation from polluted water. *Adv. Compos. Hybrid Mater.* **2022**, *5*, 1852–1864. [CrossRef]
15. Liu, D.; Chi, H.; Ma, C.; Song, M.; Zhang, P.; Dai, P. Improving in-plane and out-of-plane thermal conductivity of polyimide/boron nitride film with reduced graphene oxide by a moving magnetic field induction. *Compos. Sci. Technol.* **2022**, *220*, 109292. [CrossRef]
16. Li, L.; Zhou, B.; Han, G.; Feng, Y.; He, C.; Su, F.; Ma, J.; Liu, C. Understanding the effect of interfacial engineering on interfacial thermal resistance in nacre-like cellulose nanofiber/graphene film. *Compos. Sci. Technol.* **2020**, *197*, 108229. [CrossRef]
17. Zhao, L.; Yan, L.; Wei, C.; Wang, Z.; Jia, L.; Ran, Q.; Huang, X.; Ren, J. Aqueous-Phase Exfoliation and Functionalization of Boron Nitride Nanosheets Using Tannic Acid for Thermal Management Applications. *Ind. Eng. Chem. Res.* **2020**, *59*, 16273–16282. [CrossRef]
18. Yang, J.; Chen, Z.; Liang, L.; Guan, Z.; Ren, J. Synergistic Enhanced Thermal Conductivity and Crack Resistance of Reactor Epoxy Insulation with Boron Nitride Nanosheets and Multiwalled Carbon Nanotubes. *Nanomaterials* **2022**, *12*, 3235. [CrossRef]
19. Li, J.; Zhao, X.; Wu, W.; Zhang, Z.; Xian, Y.; Lin, Y.; Lu, Y.; Zhang, L. Advanced flexible rGO-BN natural rubber films with high thermal conductivity for improved thermal management capability. *Carbon* **2020**, *162*, 46–55. [CrossRef]
20. Yu, C.; Zhang, J.; Li, Z.; Tian, W.; Wang, L.; Luo, J.; Li, Q.; Fan, X.; Yao, Y. Enhanced Through-Plane Thermal Conductivity of Boron Nitride/Epoxy Composites. *Compos. Sci. Technol.* **2017**, *98*, 25–31. [CrossRef]
21. Yin, C.; Liu, Z.; Mo, R.; Fan, J.; Shi, P.; Xu, Q.; Min, Y. Copper nanowires embedded in boron nitride nanosheet-polymer composites with enhanced thermal conductivities for thermal management. *Polymers* **2020**, *195*, 122455. [CrossRef]
22. Su, Z.; Wang, H.; Yea, X.; Tian, K.; Huang, W.; He, J.; Guo, Y.; Tian, X. Synergistic enhancement of anisotropic thermal transport flexible polymer composites filled with multi-layer graphene (mG) and mussel-inspiring modified hexagonal boron nitride (h-BN). *Compos. Part A* **2018**, *111*, 12–22. [CrossRef]
23. Wang, T.; Tsai, J. Investigating thermal conductivities of functionalized graphene and graphene/epoxy nanocomposites. *Comput. Mater. Sci.* **2016**, *122*, 272–280. [CrossRef]
24. Cao, M.; Xiong, D.; Yang, L.; Li, S.; Xie, Y.; Guo, Q.; Li, Z.; Adams, H.; Gu, J.; Fan, T.; et al. Ultrahigh Electrical Conductivity of Graphene Embedded in Metals. *Adv. Funct. Mater.* **2019**, *29*, 1806792. [CrossRef]
25. Liu, Z.; Li, J.; Liu, X. Novel Functionalized BN Nanosheets/Epoxy Composites with Advanced Thermal Conductivity and Mechanical Properties. *ACS Appl. Mater. Interfaces* **2020**, *12*, 6503–6515. [CrossRef]
26. Cheng, L.; Feng, J. Flexible and fire-resistant all-inorganic composite film with high in-plane thermal conductivity. *Chem. Eng. J.* **2020**, *398*, 125633. [CrossRef]
27. Pan, D.; Yang, G.; Abo-Dief, H.; Dong, J.; Su, F.; Liu, C.; Li, Y.; Xu, B.; Murugadoss, V.; Naik, N.; et al. Vertically Aligned Silicon Carbide Nanowires/Boron Nitride Cellulose Aerogel Networks Enhanced Thermal Conductivity and Electromagnetic Absorbing of Epoxy Composites. *Nano-Micro Lett.* **2022**, *14*, 118. [CrossRef] [PubMed]

28. An, J.; El-Said, W.; Yea, C.; Kim, T.; Choi, J. Surface-Enhanced Raman Scattering of Dopamine on Self-Assembled Gold Nanoparticles. *J. Nanosci. Nanotechnol.* **2011**, *11*, 4424–4429. [CrossRef]
29. Shen, Y.; Li, S.; Qi, R.; Wu, C.; Yang, M.; Wang, J.; Cai, Z.; Liu, K.; Yue, J.; Guan, B.; et al. Assembly of Hexagonal Column Interpenetrated Spheres from Plant Polyphenol/Cationic Surfactants and Their Application as Antimicrobial Molecular Banks. *Angew. Chem. Int. Ed* **2022**, *61*, 2–11. [CrossRef]
30. Morishita, T.; Okamoto, H. Facile Exfoliation and Noncovalent Superacid Functionalization of Boron Nitride Nanosheets and Their Use for Highly Thermally Conductive and Electrically Insulating Polymer Nanocomposites. *ACS Appl. Mater. Interfaces* **2016**, *8*, 27064–27073. [CrossRef]
31. Wang, X.; Feng, C.; Wang, M.; Lu, H.; Ni, H.; Chen, J. Multilayered ultrahigh molecular weight polyethylene/natural graphite/boron nitride composites with enhanced thermal conductivity and electrical insulation by hot compression. *J. Appl. Polym. Sci.* **2021**, *138*, 49938. [CrossRef]
32. Wang, Z.; Liu, W.; Liu, Y.; Ren, Y.; Li, Y.; Zhou, L.; Xu, J.; Lei, J.; Li, Z. Highly thermal conductive, anisotropically heat-transferred, mechanically flexible composite film by assembly of boron nitride nanosheets for thermal management. *Compos. Part B* **2020**, *180*, 107569. [CrossRef]
33. Lin, M.; Li, Y.; Xu, K.; Ou, Y.; Su, L.; Feng, X.; Li, J.; Qi, H.; Liu, D. Thermally conductive nanostructured, aramid dielectric composite films with boron nitride nanosheets. *Compos. Sci. Technol.* **2019**, *175*, 85–91. [CrossRef]
34. Ma, T.; Zhao, Y.; Ruan, K.; Liu, X.; Zhang, J.; Guo, Y.; Yang, X.; Kong, J.; Gu, J. Highly Thermal Conductivities, Excellent Mechanical Robustness and Flexibility, and Outstanding Thermal Stabilities of Aramid Nanofiber Composite Papers with Nacre Mimetic Layered Structures. *ACS Appl. Mater. Interfaces* **2020**, *12*, 1677–1686. [CrossRef]
35. Hu, J.; Huang, Y.; Zeng, X.; Li, Q.; Ren, L.; Sun, R.; Xu, J.; Wong, C. Polymer composite with enhanced thermal conductivity and mechanical strength through orientation manipulating of BN. *Compos. Sci. Technol.* **2018**, *160*, 127–137. [CrossRef]
36. Tanimoto, M.; Yamagata, T.; Miyata, K.; Ando, S. Anisotropic thermal diffusivity of hexagonal boron nitride-filled polyimide films: Effects of filler particle size, aggregation, orientation, and polymer chain rigidity. *ACS Appl. Mater. Interfaces* **2013**, *5*, 4374–4382. [CrossRef]
37. Wu, K.; Fang, J.; Ma, J.; Huang, R.; Chai, S.; Chen, F.; Fu, Q. Achieving a Collapsible, Strong, and Highly Thermally Conductive Film Based on Oriented Functionalized Boron Nitride Nanosheets and Cellulose Nanofiber. *ACS Appl. Mater. Interfaces* **2017**, *9*, 30035–30045. [CrossRef]
38. Feng, C.; Chen, L.; Tian, G.; Bai, L.; Bao, R.; Liu, Z.; Ke, K.; Yang, M.; Yang, W. Robust polymer-based paper-like thermal interface materials with a through-plane thermal conductivity over 9 $Wm^{-1}K^{-1}$. *Chem. Eng. J.* **2020**, *392*, 123784. [CrossRef]
39. Lee, W.; Kim, J. Enhanced through-plane thermal conductivity of paper-like cellulose film with treated hybrid fillers comprising boron nitride and aluminum nitride. *Compos. Sci. Technol.* **2020**, *200*, 108424. [CrossRef]
40. Zhou, B.; Zhang, Z.; Li, Y.; Han, G.; Feng, Y.; Wang, B.; Zhang, D.; Ma, J.; Liu, C. Flexible, Robust, and Multifunctional Electromagnetic Interference Shielding Film with Alternating Cellulose Nanofiber and MXene Layers. *ACS Appl. Mater. Interfaces* **2020**, *12*, 4895–4905. [CrossRef]
41. Weng, Q.; Wang, X.; Wang, X.; Bando, Y.; Golberg, D. Functionalized hexagonal boron nitride nanomaterials: Emerging properties and applications. *Chem. Soc. Rev.* **2016**, *45*, 3989–4012. [CrossRef] [PubMed]
42. Ji, S.; Jung, H.; Kim, M.; Lim, J.; Kim, J.; Ryu, J.; Jeong, D. Enhanced Energy Storage Performance of Polymer/Ceramic/Metal Composites by Increase of Thermal Conductivity and Coulomb-Blockade Effect. *ACS Appl. Mater. Interfaces* **2021**, *13*, 27343–27352. [CrossRef] [PubMed]
43. Cai, X.; Dong, X.; Lv, W.; Ji, C.; Jiang, Z.; Zhang, X.; Gao, T.; Yue, K.; Zhang, X. Synergistic enhancement of thermal conductivity for low dielectric constant boron nitride–polytetrafluoroethylene composites by adding small content of graphene nanosheets. *Compos. Commun.* **2020**, *17*, 163–169. [CrossRef]
44. He, B.; Lau, S.; Chan, H.; Fan, J. High dielectric permittivity and low percolation threshold in nanocomposites based on poly(vinylidene fluoride) and exfoliated graphite nanoplates. *Adv. Mater.* **2009**, *21*, 710–715. [CrossRef]
45. Shi, X.; Wang, K.; Tian, J.; Yin, X.; Guo, B.; Xi, G.; Wang, W.; Wu, W. Few-Layer Hydroxyl-Functionalized Boron Nitride Nanosheets for Nanoscale Thermal Management. *ACS Appl. Nano Mater.* **2020**, *3*, 2310–2321. [CrossRef]
46. Tong, Z.; Liu, M.; Bao, H. A numerical investigation on the heat conduction in high filler loading particulate composites. *Int. J. Heat Mass Transf.* **2016**, *100*, 355–361. [CrossRef]